PERGAMON

International Journal of Heat and Mass Transfer 44 (2001) 3385–3395

International Journal of HEAT and MASS TRANSFER

www.elsevier.com/locate/ijhmt

Local heat transfer around a wall-mounted cube in the turbulent boundary layer

Hajime Nakamura *, Tamotsu Igarashi, Takayuki Tsutsui

Department of Mechanical Engineering, National Defense Academy, Hashirimizu 1-10-20, Yokosuka, Kanagawa 239-0811, Japan

Received 3 March 2000; received in revised form 8 December 2000

Abstract

Experimental studies were performed to investigate the fluid flow and local heat transfer around a cube mounted on a wall of a plane. The Reynolds number based on the cube height ranged from 4.2×10^3 to 3.3×10^4. The turbulent boundary layer thickness δ was 1.5–1.83 times higher than the cube height d. Surface temperatures on the cube and the base wall were measured directly with numerous thermocouples under the condition of constant heat flux. In the present paper, local heat transfer characteristics on the cube and the base wall were clarified correlating to the flow characteristics. In the range of the present Reynolds number, the overall Nusselt number of the cube can be expressed by $Nu_m = 0.137 Re^{0.68}$.

1. Introduction

The objective of the present study is to accumulate the basic data about the cooling design of electric equipment. As simple models of the practical equipment, two-dimensional blocks of actual size of electric equipment were arranged in line on a flat plate. Igarashi and Yamasaki [1] reported the fluid flow and local heat transfer of a two-dimensional rectangular block in the turbulent boundary layer on a plate. Igarashi and Takasaki [2,3] presented the interaction characteristics between the height of a block and the thickness of a laminar boundary layer by using three two-dimensional rectangular blocks arranged in line. Additionally, the local and average heat transfer on every face of the second block was investigated and discussed in connection with the characteristics of the flow around the blocks. Igarashi and Takasaki [4] studied a two-dimensional block in a laminar flat-plate boundary layer. Introducing a new reference length, the average Nusselt numbers on each face are generally correlated to Reynolds number and the width/height ratio of the rectangular block. And Igarashi [5] reported that the enhancement of heat transfer around a rectangular block on a flat plate was obtained by the transition from laminar to turbulent flow by a tripping wire attached on the flat-plate upstream of the block.

The most simple three-dimensional model is a cube or a circular block with height/diameter < 1 or a square block with height/side length < 1. Chyu and Natarajan [6] studied the local heat/mass transfer distributions on the surface of a wall-mounted cube by the naphthalene sublimation technique. The ratio of turbulent boundary layer thickness δ and the cube height d is $\delta/d = 0.2$ to 0.25 and the Reynolds number ranged from 3.1×10^4 to 1.04×10^5. Natarajan and Chyu [7] reported the effect of angle of attack on the local heat/mass transfer of the cube under the same conditions. However, the Reynolds number range in the above investigations [6,7] was much higher than that of practical electric equipment. Sato et al. [8] investigated the flow and heat transfer around a square block with a height/side length of 14/21 and an attack angle of 45°. They measured the three-dimensional flow by LDV and the surface temperatures on the block with nine thermocouples per face. Park and Nakayama [9] studied the heat transfer of a square block with height/side length = 7/31, mounted on the floor of a parallel-plate channel. Recently, Meinders et al. [10] reported the local heat transfer of a cube mounted on the floor of a parallel-plate channel. The ratio of the

* Corresponding author. Fax: +81-468-44-5900.
E-mail address: nhajime@nda.ac.jp (H. Nakamura).

0017-9310/01/$ - see front matter
PII: S0017-9310(01)00009-6

Nomenclature

Cp	pressure coefficient $=(p-p_0)/0.5\rho u_0^2$
d	cube height
h	local heat transfer coefficient $\dot{q}/(\theta_w-\theta_0)$
$\bar{h}$	average heat transfer coefficient on each face of a cube
Nu	local Nusselt number $=hd/\lambda$
$\overline{Nu}$	average Nusselt number on each face of a cube $=\bar{h}d/\lambda$
Nu_0	Nusselt number on the floor far from a cube
Nu_m	overall Nusselt number of a cube
p_0	static pressure at free-stream
p	static pressure on a wall
$\dot{q}$	heat flux
Re	Reynolds number $=u_0d/v$
$\bar{u}$	time-averaged velocity
Δu	root mean square value of fluctuating velocity
u^*	friction velocity $=\sqrt{\tau_0/\rho}$
u_0	free-stream velocity
x,y,z	streamwise, vertical and cross-stream coordinates
δ	boundary layer thickness
θ_0,θ_w	free-stream temperature and wall temperature
λ	thermal conductivity of fluid
v,ρ	kinematic viscosity and density of fluid
τ_0	shear stress

Subscripts

f, s, r, t front, side, rear, top faces

cube height d and the channel height D was $d/D=0.3$. The boundary layer was developing turbulence and the Reynolds number based on the cube height ranged from 2.75×10^3 to 4.97×10^3. The surface temperature of an internally heated cubical element was measured with infrared thermography.

From a review of the foregoing literature dealing with a three-dimensional prism [6–10], the turbulent boundary layer thickness was usually lower than the height of the prism, and little attention has been given to the heat transfer of the base wall around the prism. Hence, the authors investigate on the local heat transfer distributions of a cube and the base wall under the higher turbulent boundary layer thickness than the cube height ($\delta/d=1.5$ to 1.83). The Reynolds number based on the cube height ranged from 4.2×10^3 to 3.3×10^4, because no results have been reported on the local heat transfer of the cube in this Reynolds number range. The surface temperatures were measured directly by numerous thermocouples. Flow characteristics were also investigated by surface pressure measurements and flow visualizations. The local heat transfer characteristics were correlated to the flow characteristics.

2. Experimental apparatus and procedure

Fig. 1 shows a coordinate system with respect to the wall-mounted cube. Experiments were conducted in a low-speed wind tunnel with a working section 400 mm high, 300 mm wide and 800 mm long. A cube, with height d of 30 mm, was mounted on the floor of the wind tunnel. The free-stream velocity u_0 ranged from 2.2 to 17.3 m/s, therefore the Reynolds number based on the cube height ranged from $Re=4.2\times10^3$ to 3.3×10^4. The turbulent intensity of the free-stream in this range was about 0.5%. The turbulent boundary layer was achieved by attaching a circular cylinder of 10 mm in diameter on the floor at 500 mm upstream from the cube. The boundary layer thickness δ ranged from 45 to 55 mm at the position of the cube's leading edge, therefore the ratio δ/d ranged from 1.5 to 1.83. Fig. 2(a) shows the mean velocity distributions in the turbulent boundary layer for different free-stream velocities. The friction velocity u^* was deduced from the following relationship [11]:

$$u^{*2}=\frac{\tau_0}{\rho}=0.0225\,u_0^{7/4}\left(\frac{v}{\delta}\right)^{1/4}. \tag{1}$$

A solid line in Fig. 2(a) denotes the experimental universal velocity distribution on a flat-plate turbulent boundary layer at zero pressure gradient [11] expressed as:

$$\frac{\bar{u}}{u^*}=5.85\log\left(\frac{yu^*}{v}\right)+5.56. \tag{2}$$

The velocity distributions at $u_0=2.2$ and 4.1 m/s agree well with Eq. (2) although the velocities at $u_0=8.3$ and 16.6 m/s are somewhat higher within 7% than Eq. (2). Fig. 2(b) shows the distributions of root mean square values of fluctuating velocity in the turbulent boundary

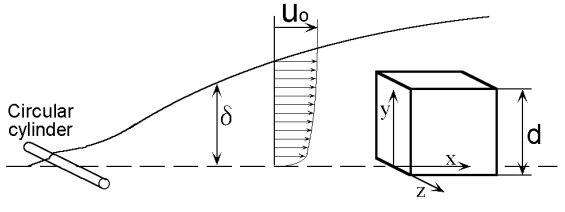

Fig. 1. Coordinate system and symbols.

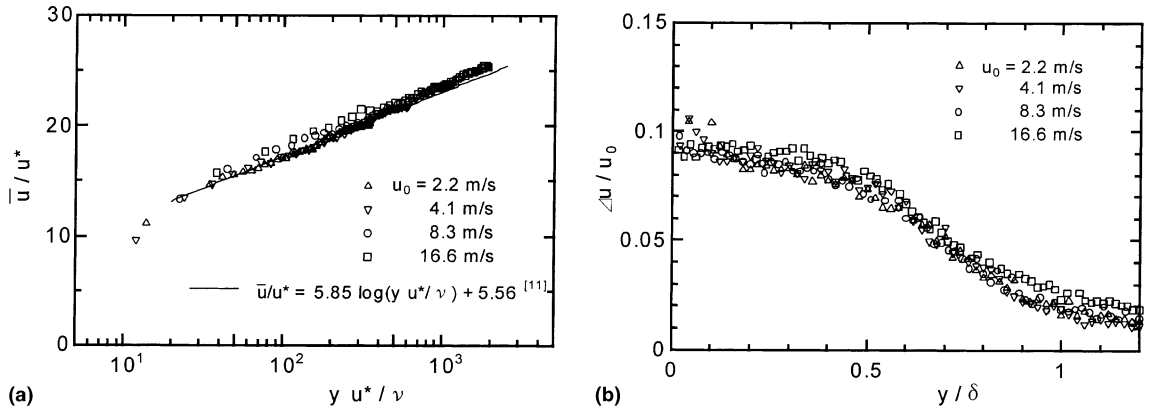

Fig. 2. Velocity distributions in the turbulent boundary layer for different free-stream velocities: (a) mean velocity; (b) fluctuating velocity.

layer. A similar profile is shown for the different free-stream velocities.

The visualization of the surface flow on the floor and the cube was made using an oil-film method. The surface pressures on the floor and the cube were measured by inclined multi-tube manometers connected with pressure taps of 0.6 mm in diameter, at 4 mm intervals on the cube faces, and 2.5–10 mm intervals on the floor.

Figs. 3(a) and (b) show the test model for the local heat transfer measurement. The cube and the floor were fabricated from acrylic resin plates of 3 and 5 mm in thickness, respectively. The faces of the cube and the floor were covered with five stainless steel sheets of 0.02 mm in thickness and 30 mm in width. One sheet covered three faces of the cube and floor, and the others covered the floor. They were connected in series electrically and heated by applying an alternating current under the condition of constant heat flux. The temperature difference between the heated surface and the free-stream was about 10°C. The radiant energy can be neglected in the estimation of the heat transfer. Copper–constantan thermocouples of 0.1 mm in diameter were attached underneath the stainless steel sheets in one-fourth of the entire surface area, at 3 mm intervals on the cube surfaces, and 4–8 mm intervals on the floor. In order to obtain the temperatures over the entire area, measurements were performed four times under the same experimental condition by rotating the cube every 90° along the axis parallel to the vertical coordinate.

To estimate the heat loss by conduction from the heater to the acrylic resin, the thermocouples were also attached on interior surfaces of the cube, under surface of the base wall and unheated faces of the cube. The heat loss was calculated using a heat conduction analysis. The effect of conduction along the thermocouple leads on the temperature measurement was also estimated using the method presented by Satyamurthy et al. [12]. The sum of the above losses on the cube was 19.8% for $u_0 = 17.3$ m/s, and 28.5% for $u_0 = 2.2$ m/s, compared with the heat input from the heater. These were mainly due to the conduction to the unheated faces. The heat transfer coefficient was calculated taking the above losses into account.

The experimental uncertainties were calculated using standard uncertainty analysis methods proposed by Kline [13]. The uncertainty of the temperature difference

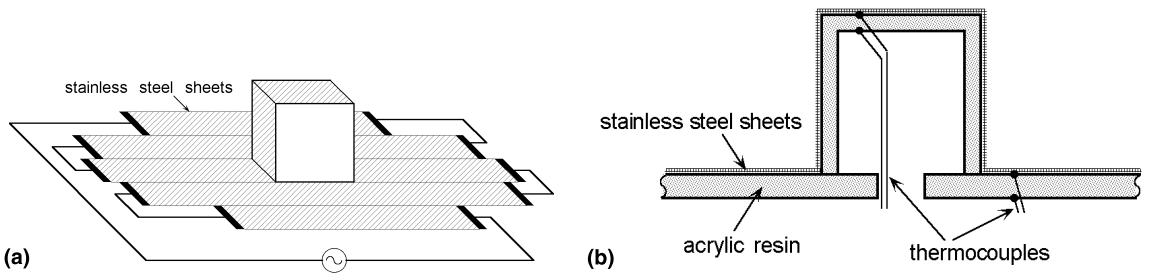

Fig. 3. Experimental model for local heat transfer measurement: (a) exterior view; (b) cross-sectional view.

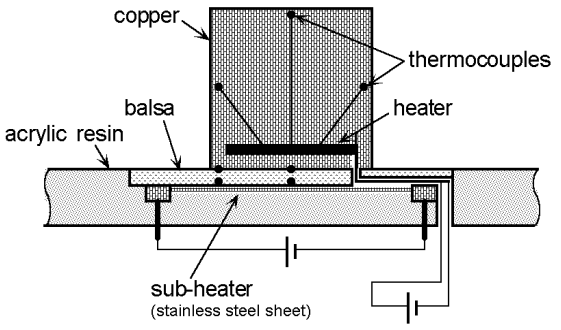

Fig. 4. Experimental model for overall heat transfer measurement.

between the wall and free-stream ranged from 1% to 2% depending on the wall temperature, and the uncertainty of the input of surface heat flux was 1%. The uncertainty of the heat losses was within 5% to the heat input. This was derived from the dispersion generated by various assumption of temperature distribution between the measured points. The total uncertainty for the heat transfer coefficient was within 5.5%.

In order to verify the measurement of the local heat transfer obtained from the above constant heat flux model, overall heat transfer of the cube was measured by a constant temperature model and compared with that obtained from the constant heat flux model. Fig. 4 shows the constant temperature model. A cube, with height d of 30 mm, was fabricated from copper and heated by a heater buried in it. The surface temperature of the heated cube was constant within ± 0.05°C and was higher by about 6°C than the free-stream temperature. In order to prevent heat losses to the base wall and the leads, a balsa wood sheet of 3 mm in thickness was covered under the cube. Moreover, a stainless steel sheet was set under the balsa sheet, as a sub-heater, and it was heated to maintain zero temperature gradient between the cube and the sub-heater. The uncertainty of the measured temperature difference between the wall and free-stream was 0.8%, and the uncertainty of heat input was 0.2%. The uncertainty of the heat loss estimated by the temperature difference between the cube and the sub-heater was within 0.6%. The total uncertainty for the overall heat transfer coefficient was within 1.1%.

3. Fluid flow around a cube

3.1. Surface oil-flow pattern

Figs. 5(a) and (b) show the typical surface oil-flow patterns around the cube, top view and unfolding view, respectively. The sketches of surface flow obtained by the oil-flow patterns and smoke visualizations are shown in Figs. 6(a) and (b). On the floor, a horseshoe pattern is formed in front of and on both side regions of the cube. The size of the horseshoe vortex region defined by the flow separation line seen in the oil-flow pattern is $d/3$ in the front and $d/2$ on both side regions. This fact is almost the same as that reported by Martinuzzi and Tropea [14] under the condition of fully developed

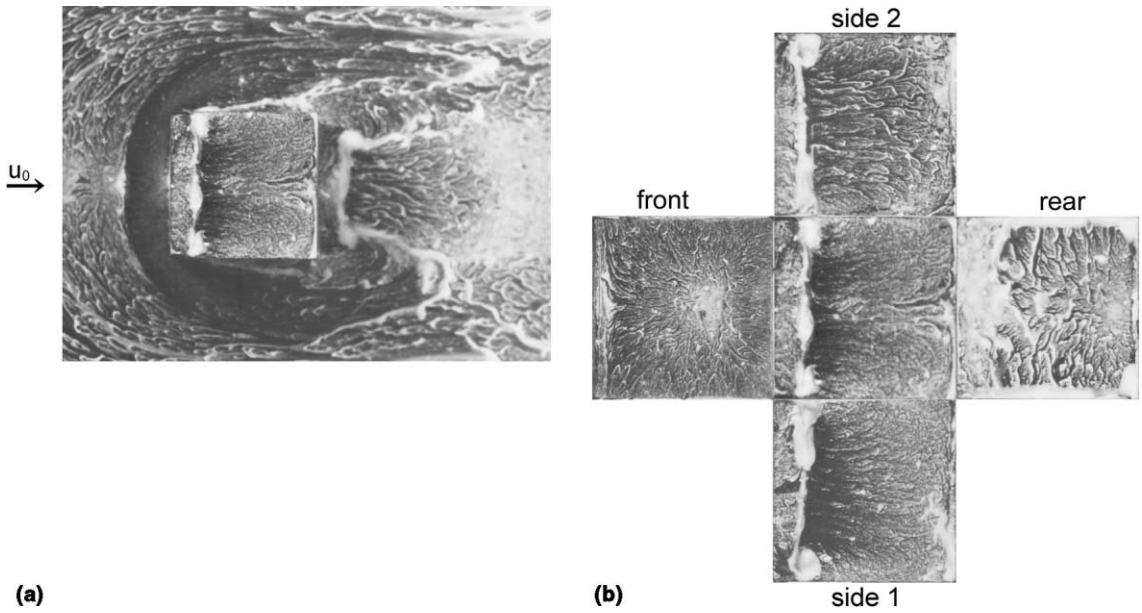

Fig. 5. Surface oil-film pattern around a cube, $u_0 = 16$ m/s, $Re = 3.1 \times 10^4$: (a) top view; (b) cube.

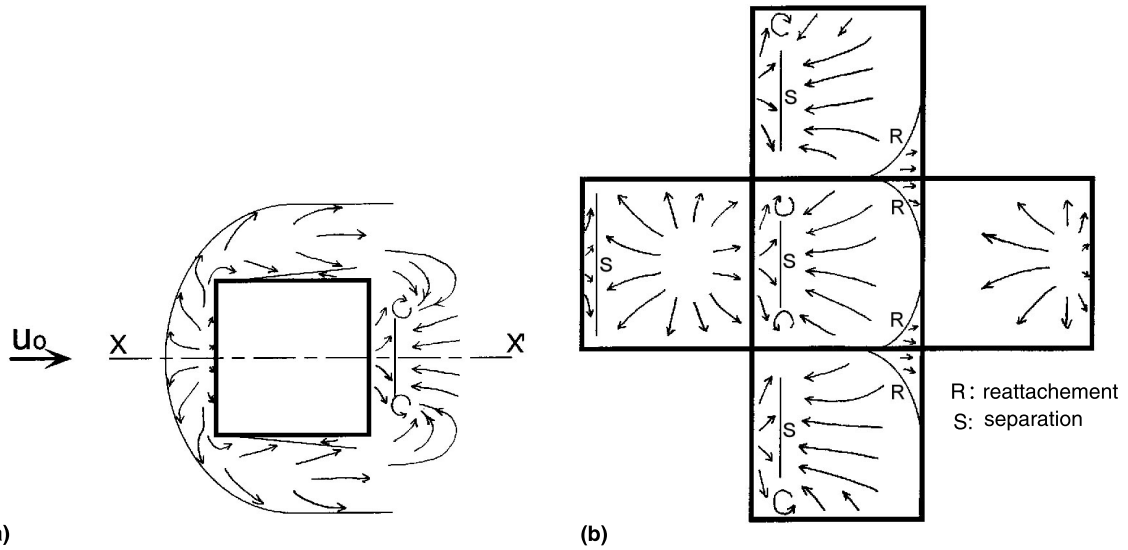

Fig. 6. Sketches of surface flow pattern, $Re = 3.1 \times 10^4$: (a) floor; (b) cube.

channel flow. On the front face of the cube, the front stagnation point is $z = 0$, $y/d = 0.6$ and the flow is spread radially. In the bottom part of the front face, a secondary vortex is seen. The shear layers separated from both sides and the upper edges on the front face reattach onto around the backward edges on both side faces and the top face, respectively. Reverse flows appear on both side faces and the top face, and separate at the upstream regions of $x/d = 1/6$. On the rear face, an upward flow is formed at $y/d > 0.15$. The sketch of flow along the center line of $z = 0$ is shown in Fig. 7.

3.2. Pressure distributions

Figs. 8(a) and (b) show the contours of the mean pressure coefficient on the floor and the cube, respectively. The uncertainty level of the pressure coefficient Cp associated with the measurement method was ± 0.01. On the floor, there is a high pressure region in front of the cube ($x/d = -0.1$, $z = 0$) due to flow reattachment (see Fig. 7). Minimum values of Cp exist downstream of corners A and D ($x/d = 0.2$, $z/d = \pm 0.6$) due to the flow separation at these corners. The pressure distribution on the floor is similar to that obtained by Martinuzzi and Tropea [14]. The position of the maximum value of Cp on the front face of the cube coincides with the stagnation point at $z = 0$, $y/d = 0.6$. On both side, top and rear faces, the values of Cp are all negative, because these faces are in the separated flow region. The value of Cp is maximum at each reattachment region on both side faces and top face, and decreases along the direction of reverse surface flow.

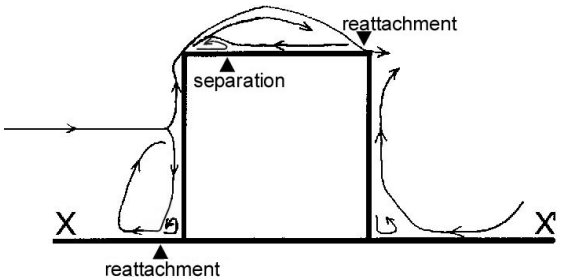

Fig. 7. Sketch of flow along center line ($z = 0$), $Re = 3.1 \times 10^4$.

4. Heat transfer characteristics

4.1. Local heat transfer

Contours of the local Nusselt number around the cube at $Re = 3.3 \times 10^4$ are shown in Figs. 9(a) and (b). On the floor, the Nusselt number in the horseshoe vortex region is remarkably high, in that it is about three times as high as that on the floor far from the cube ($Nu_0 = 100$). On the front face of the cube, the Nusselt number distribution is almost flat along the vertical direction except near the upper and bottom corners and it increases toward both side edges. On both side faces and the top face, the values of Nusselt number have maximums in the flow reattaching regions near the backward edges, and decrease along the direction of reverse flow. The value of Nusselt number on the rear face is considerably lower than that of other faces. Figs. 10(a) and (b) show the case of low Reynolds number $Re = 4.2 \times 10^3$. Although the Nusselt number on the floor is high in the region of the horseshoe vortex, the high Nusselt number region more

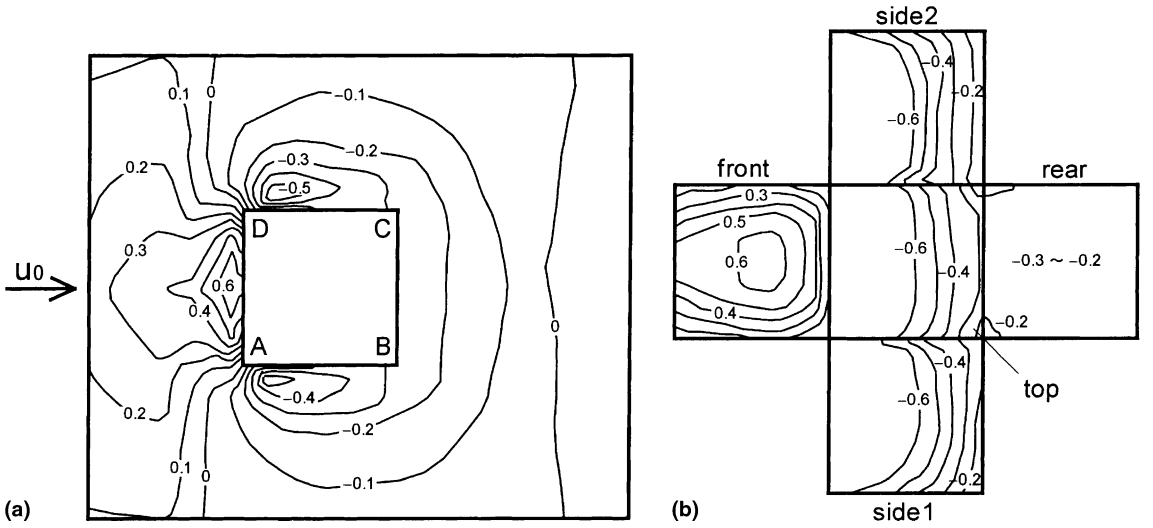

Fig. 8. Pressure coefficient contours around a cube, $Re = 3.1 \times 10^4$: (a) floor; (b) cube.

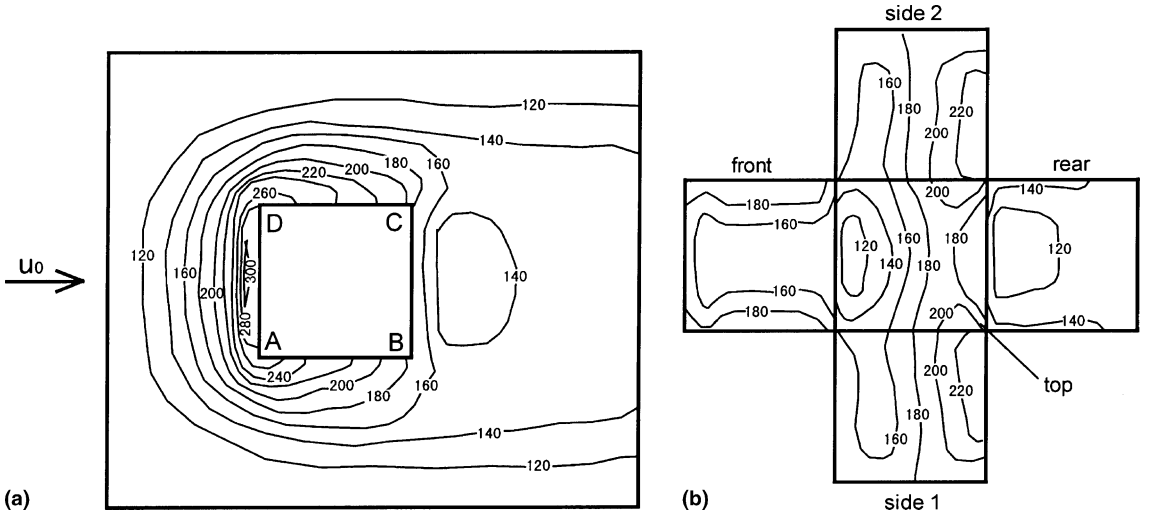

Fig. 9. Local Nusselt number contours around a cube, $Re = 3.3 \times 10^4$: (a) floor; (b) cube.

than double of $Nu_0 = 25$ is seen only in front of the cube, not extending to both side regions. At the higher Reynolds number $Re = 3.3 \times 10^4$, the maximum Nusselt number in the horseshoe vortex region is nearly double than that at the center line of $z = 0$ on the front face of the cube. On the other hand, at $Re = 4.2 \times 10^3$, the maximum Nusselt number in the horseshoe vortex region is a little higher than the value at the center line of $z = 0$ on the front face.

The Nusselt number distributions on each face for given heights (y/d) at $Re = 3.3 \times 10^4$ are presented in Fig. 11. The profiles of the individual faces have distinctive features, but the profiles for various heights resemble each other. Each profile on the front face overlaps in the range of $0.1 < y/d < 0.9$. On both side faces, the values of Nusselt number decrease from the backward edges B and C to front edges A and D, respectively, and have minimums at the separation point of the reverse flow. Near the backward edges on both side faces, the values of Nusselt number in the upper part are higher than those in the bottom part. On the front and rear faces, the values of Nusselt number near the side edges are higher than those in the central part. This is caused by a cut-off of the thermal boundary layer at the edges of the faces. Fig. 12 shows the variation of local Nusselt number distributions with Reynolds number at the height of $y/d = 0.5$. The value of Nusselt number on the rear

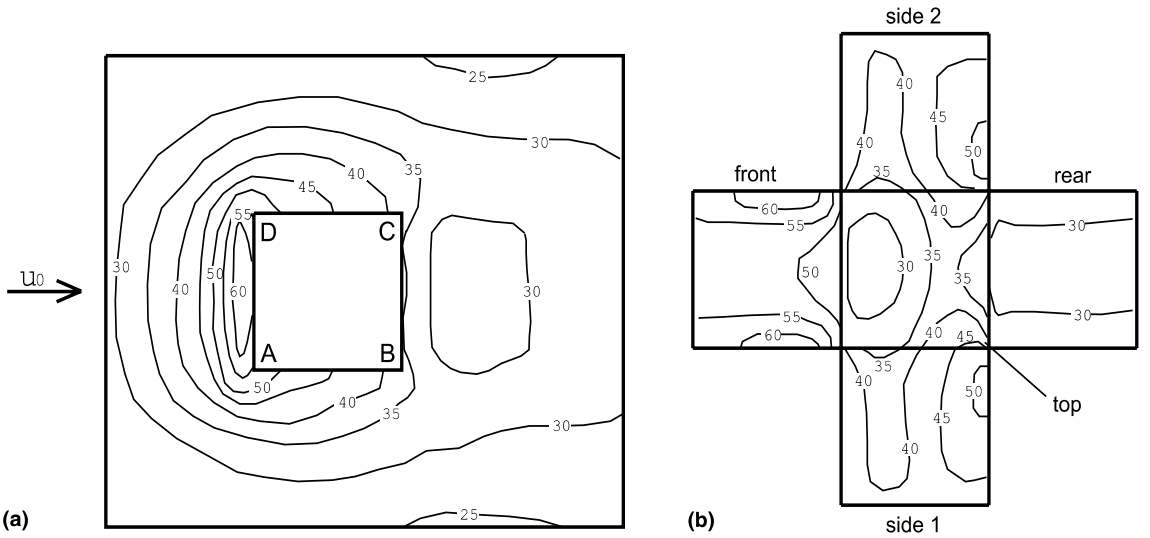

Fig. 10. Local Nusselt number contours around a cube, $Re = 4.2 \times 10^3$: (a) floor; (b) cube.

face is lower than that on other faces in the range of the present Reynolds number. At the lower Reynolds number, the value of Nusselt number on the front face is high compared with that on other faces. At the higher Reynolds number, the maximum Nusselt numbers near the backward edges on both side faces (B and C) become clear.

Fig. 13(a) shows the Nusselt number distribution at $y/d = 0.5$ for $Re = 3.3 \times 10^4$ compared with that of two-dimensional square prism obtained by Igarashi [15,16]. On the front and both side faces, the value of Nusselt number of the cube is higher than that of square prism. This difference mainly depends on the heat transfer enhancement by the horseshoe vortex formed in front of and on both side regions of the cube. On the contrary, the value on the rear face is lower than that of square prism. Fig. 13(b) shows the comparison of the Nusselt number distribution at $y/d = 0.5$ for $Re = 4.2 \times 10^3$ with that obtained by Meinders et al. [10]. On both side faces, minimum values of the Nusselt number exist in almost the same position as those of Meinders et al., and they increase in both backward and forward directions. Although the minimum values of the Nusselt number obtained by Meinders et al. are much lower than the present experiment. This difference may be caused by the different flow condition, the flat-plate turbulent boundary layer for the present experiment and the developing turbulent flow in the parallel channel for Meinders et al. The separation bubble on the side face for Meinders et al. is thought to be more stationary, and the increased air temperature in the separation bubble caused a decrease in the minimum heat transfer. Near edges of the cube, the heat transfer obtained by Meinders et al. shows extremely low values. But in the present experiment, there is no extreme change in the Nusselt number near the edges.

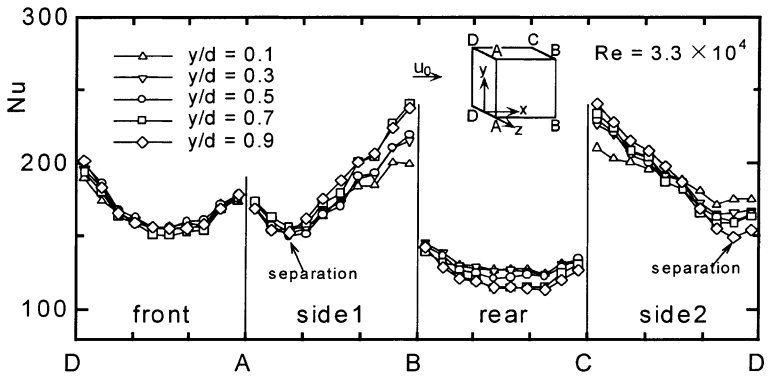

Fig. 11. Local Nusselt number distributions around a cube for various height of y/d at $Re = 3.3 \times 10^4$.

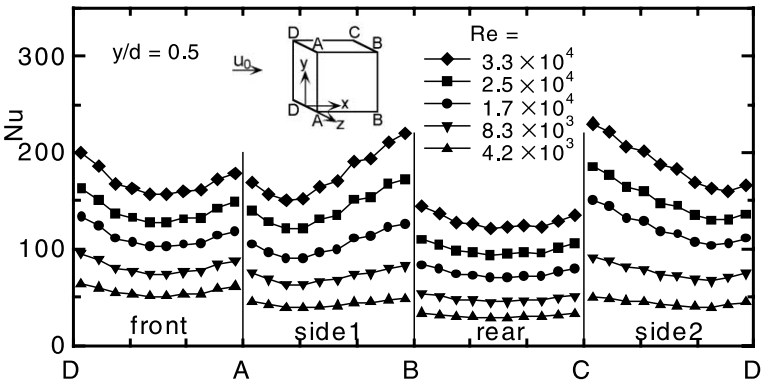

Fig. 12. Variation of local Nusselt number distributions around a cube with Reynolds number at the height of $y/d = 0.5$, $Re = 4.2 \times 10^3$ to 3.3×10^4.

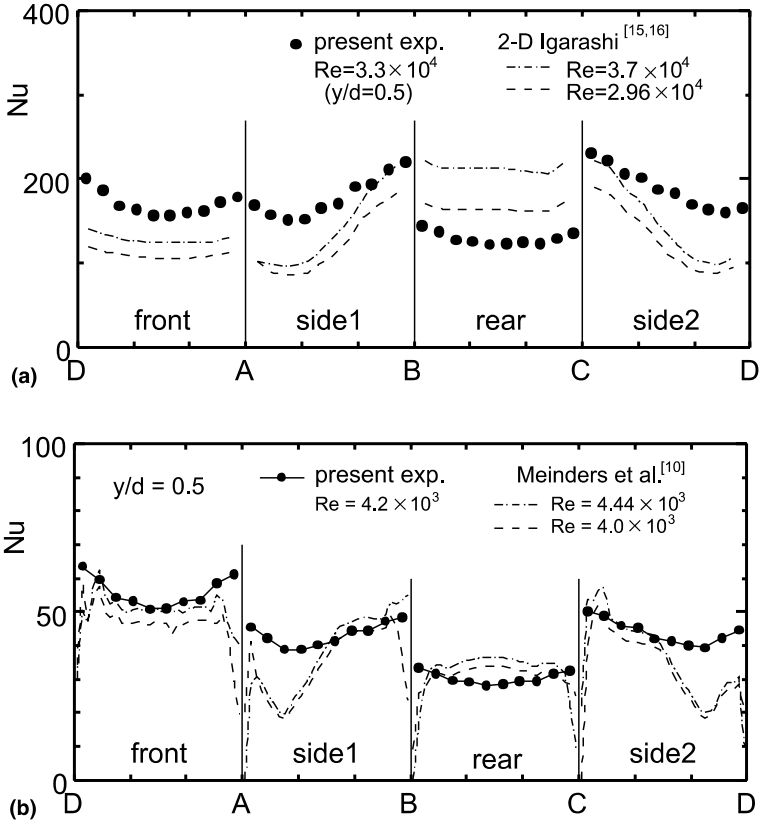

Fig. 13. Comparison of local Nusselt number distributions with that of other researchers: (a) comparison with that of a two-dimensional square prism; (b) comparison with that of a wall-mounted cube by Meinders et al.

The streamwise Nusselt number distributions for a given transverse location (z/d) at $Re = 3.3 \times 10^4$ are presented in Fig. 14. The Nusselt number is the averaged value between $+z/d$ and $-z/d$. On the floor in front of the cube, the value of Nusselt number increases with decreased distance of the cube due to the enhancement of heat transfer by the horseshoe vortex. On the front face of the cube, Nusselt number distributions in the vertical direction are almost flat. According to Meinders et al. [10], vertical distribution of the heat transfer

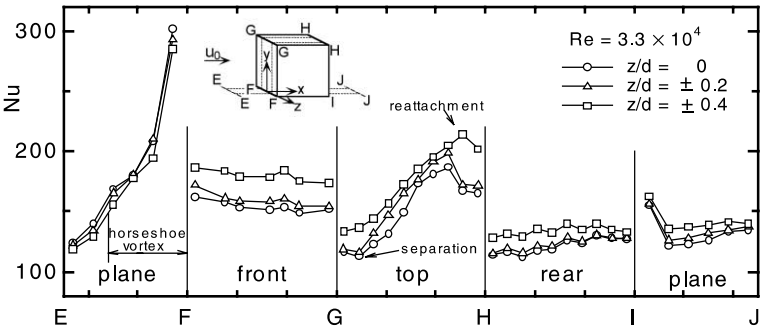

Fig. 14. Streamwise local Nusselt number distributions for various transverse location of z/d at $Re = 3.3 \times 10^4$.

coefficient on the front face is also almost flat in the range of $0.2 < y/d < 0.8$. On the other hand, according to Chyu and Natarajan [6], vertical distribution of the Sherwood number Sh on the front face is almost flat over $0.3 < y/d < 0.8$, but the values of Sh at $y/d > 0.8$ and $y/d < 0.1$ are 50% higher and the value at $0.1 < y/d < 0.2$ is 20% lower than that of the center part. On the top face, the value of Nusselt number has a maximum in the reattachment region of the shear layer separated from the front edge G. Near the side edges ($z/d = \pm 0.4$), the value of Nusselt number is higher than that in the central part ($z = 0$). The value of Nusselt number decreases toward upstream and has a minimum at the separation point of the reverse flow. On the rear face, the Nusselt number decreases along the upward flow. Fig. 15 shows the variation of the streamwise local Nusselt number distributions with Reynolds number at $z = 0$. The maximum Nusselt number on the floor in front of the cube increases remarkably with an increase in Reynolds number. On the top face, the maximum value in the reattachment region becomes clear with an increase in Reynolds number. The minimum Nusselt number region on the top face corresponding to the separation point of the reverse flow moves backward with a decrease in Reynolds number and is $x/d = 1/4$ from the edge G at $Re = 4.2 \times 10^3$.

4.2. Average heat transfer on each face

Fig. 16 shows the face-averaged Nusselt number with the Reynolds number on the front, side, rear and top faces of the cube. The value of Nusselt number on the side face is the averaged value of both side faces. The correlation of the Nusselt number on each face can be expressed as

$$\text{Front face}: \quad \overline{Nu_f} = 0.71\,Re^{0.52}, \tag{3}$$

$$\text{Side face}: \quad \overline{Nu_s} = 0.12\,Re^{0.70}, \tag{4}$$

$$\text{Rear face}: \quad \overline{Nu_r} = 0.11\,Re^{0.67}, \tag{5}$$

$$\text{Top face}: \quad \overline{Nu_t} = 0.071\,Re^{0.74}. \tag{6}$$

In the range of $Re < 2 \times 10^4$, the average Nusselt number on individual faces becomes lower in the order of the front, side, top and rear faces. The exponent of Reynolds number on the front face is 0.52, which is almost equal to 0.5 on a face in laminar flow. On the other faces in the separated flow region, the exponent rises to 0.67–0.74. These results are compared with those of Chyu and Natarajan [6] and Meinders et al. [10]. The Sherwood number obtained by Chyu and Natarajan is

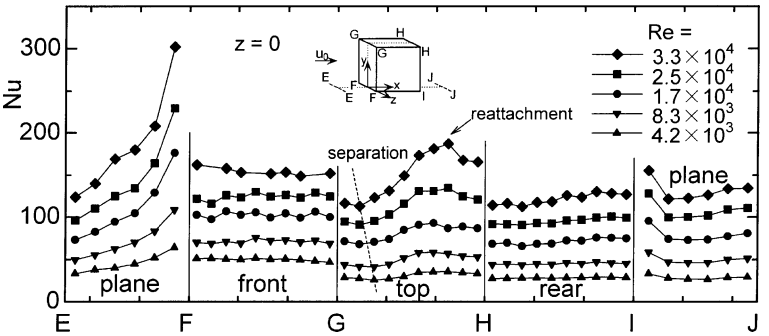

Fig. 15. Variation of streamwise local Nusselt number distributions with Reynolds number along center line ($z = 0$), $Re = 4.2 \times 10^3$ to 3.3×10^4.

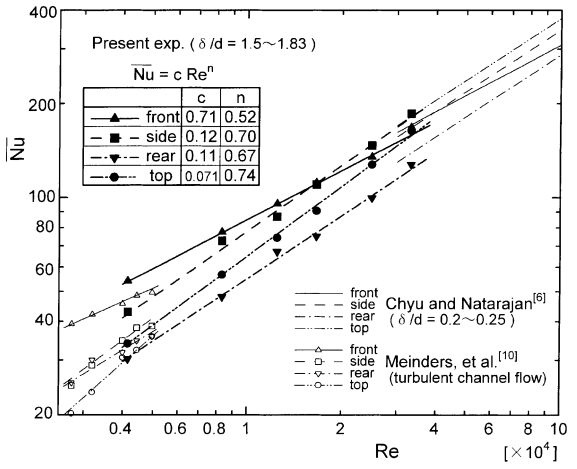

Fig. 16. Average Nusselt number on each face of a wall-mounted cube.

transformed into a Nusselt number using an analog relationship between heat and mass transfer as follows:

$$Nu/Sh = (\mathrm{Pr}/Sc)^n, \tag{7}$$

where Sc is the Schmidt number. According to Chyu and Natarajan [6], Schmidt number and the exponent n are determined to be $Sc = 1.87$ and $n = 1/3$, respectively. As shown in Fig. 16, the Nusselt number on each face obtained in the present measurement agrees with that for Chyu and Natarajan and for Meinders et al. within ±10%.

The overall Nusselt number of the cube is shown in Fig. 17. The Nusselt number obtained by the constant temperature model, as shown in Fig. 4, is also plotted to verify the value obtained by the constant heat flux model. Both Nusselt numbers agree well within ±2%. The correlation between the overall Nusselt number and the Reynolds number can be expressed as

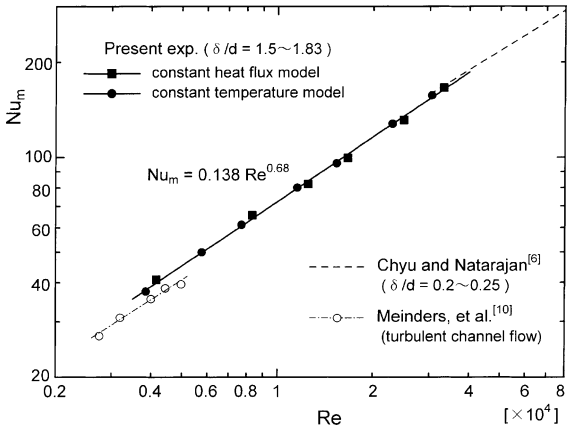

Fig. 17. Overall Nusselt number of a wall-mounted cube.

$$\text{Overall}: \quad Nu_\mathrm{m} = 0.138\,Re^{0.68} \quad (Re = 4.2\times10^3 \text{ to } 3.3\times10^4). \tag{8}$$

This correlation is almost the same as that by Chyu and Natarajan [6] at $Re = 3.3\times10^4$ and 10% higher than that by Meinders et al. [10] at $Re = 4.2\times10^3$.

5. Conclusions

Experimental studies were performed on the fluid flow and the local heat transfer around a wall-mounted cube in the turbulent boundary layer. The Reynolds number based on d ranged from 4.2×10^3 to 3.3×10^4. The main results are as follows.

1. On the base wall, the local heat transfer is remarkably high in the region of the horseshoe vortex formed in front of and on both side regions of the cube. In particular, the Nusselt number near the front face of the cube has a maximum value, that is more than double that on the base wall far from the cube.
2. On both side faces and top face of the cube, the local heat transfer has a maximum in the flow reattaching regions near the backward edges, and decreases along the direction of reverse flow on these faces. It has a minimum at the separation points of the reverse flow. On the front face, the heat transfer is almost constant along the vertical direction and it increases toward both side edges. On the rear face, the heat transfer is considerably low compared with the other faces.
3. The average Nusselt number on each face and the overall Nusselt number of the cube can be expressed as follows:

$$\text{Front face}: \quad \overline{Nu_\mathrm{f}} = 0.71\,Re^{0.52},$$

$$\text{Side face}: \quad \overline{Nu_\mathrm{s}} = 0.12\,Re^{0.70},$$

$$\text{Rear face}: \quad \overline{Nu_\mathrm{r}} = 0.11\,Re^{0.67},$$

$$\text{Top face}: \quad \overline{Nu_\mathrm{t}} = 0.071\,Re^{0.74},$$

$$\text{Overall}: \quad Nu_\mathrm{m} = 0.138\,Re^{0.68}.$$

On the front face, the exponent of Reynolds number is 0.52, that is almost equal to 0.5 on a face in laminar flow. On the other faces in the separated flow region, the exponent rises to 0.67–0.74.

References

[1] T. Igarashi, H. Yamasaki, Fluid flow and heat transfer of a two-dimensional rectangular block in the turbulent layer on a plate, in: Proceedings of the Third ASME/JSME Thermal Engineering Joint Conference, 1991, vol. 1, pp. 341–347.

[2] T. Igarashi, H. Takasaki, Fluid flow around three rectangular blocks in a flat-plate laminar boundary layer, Exp. Heat Transfer 5 (1992) 17–31.
[3] T. Igarashi, H. Takasaki, Heat transfer around three rectangular blocks in a flat-plate laminar boundary layer, in: Proceedings of the International Symposium on Turbulence, Heat and Mass Transfer, Lisbon, Portugal, 1994, vol. 1, pp. 5.2.1–5.2.6.
[4] T. Igarashi, H. Takasaki, Fluid flow and heat transfer around a rectangular block fixed on a flat-plate laminar boundary layer, in: Proceedings of the Fourth ASME/JSME Thermal Engineering Joint Conference, Maui, Hawaii, 1995, vol. 1, pp. 295–302.
[5] T. Igarashi, Enhancement of heat transfer around a rectangular block fixed on a flat-plate laminar boundary layer, in: Proceedings of the Third KSME/JSME Thermal Engineering Conference, Kyngju, Korea, 1996, vol. 1, pp. 541–546.
[6] M.K. Chyu, V. Natarajan, Local heat/mass transfer distributions on the surface of a wall-mounted cube, Trans. ASME J. Heat Transfer 113 (1991) 851–857.
[7] V. Natarajan, M.K. Chyu, Effect of flow angle-of-attack on the local heat/mass transfer from a wall-mounted cube, Trans. ASME J. Heat Transfer 116 (1994) 552–560.
[8] H. Sato, K. Hishida, M. Maeda, Turbulent flow and heat transfer characteristics around a square prism in a boundary layer, Trans. Jpn. Soc. Mech. Eng. 58 (545) (1992) 22–30 in Japanese.
[9] S.H. Park, W. Nakayama, Conjugate-mode heat transfer from a module on the floor of a parallel-plate channel to forced convective air flow (Experimental determination of macroscopic thermal conductance), Trans. Jpn. Soc. Mech. Eng. 61 (583) (1995) 1070–1077 in Japanese.
[10] E.R. Meinders, K. Hanjalic, R.J. Martinuzzi, Experimental study of the local convection heat transfer from a wall-mounted cube in turbulent channel flow, Int. J. Heat Mass Transfer 121 (1999) 564–573.
[11] H. Schlichting, Boundary Layer Theory, sixth ed., McGraw-Hill, New York, 1968, pp. 598–602.
[12] P. Satyamurthy, R.K. Marwah, N. Venkatramani, V.K. Rohatgi, Estimation of error in steady-state temperature measurement due to conduction along the thermocouple leads, Int. J. Heat Mass Transfer 22 (1979) 1151–1154.
[13] S.J. Kline, The purposes of uncertainty analysis, Trans. ASME J. Fluid Eng. 107 (1985) 153–160.
[14] R. Martinuzzi, C. Tropea, The flow around surface-mounted, prismatic obstacles places in a fully developed channel, Trans. ASME J. Fluid Eng. 115 (1993) 85–92.
[15] T. Igarashi, Heat transfer from a square prism to an air stream, Int. J. Heat Mass Transfer 28 (1) (1985) 175–181.
[16] T. Igarashi, Local heat transfer from a square prism to an airstream, Int. J. Heat Mass Transfer 29 (5) (1986) 777–784.